Applied Chemistry Today **19(73)** (2024) 123-138

Semnan University

Applied Chemistry Today

Journal homepage: https://chemistry.semnan.ac.ir/

ISSN: 2981-2437

Research Article

Fe_3O_4@SiO_2 Magnetic Core-Shell Nanoparticles Functionalized with 1,4-dihydroxyanthraquinone as an Effective and Recyclable Adsorbent for Removal of Copper Ion from Aqueous Solutions

Majid Ghahraman Afshar[a,*], Mahsa Rajabi[b], Mahmood Payehghadr[b], Niloufar Bahrami Panah[b]

[a]*Chemistry and Process Research Department, Niroo Research Institute (NRI), Tehran, Iran*
[b]*Department of Chemistry, Payame Noor University, Tehran, Iran*

PAPER INFO

Article history:
Received: 11/Jan/2024
Revised: 20/Jul/2024
Accepted: 04/Aug/2024

Keywords:
Fe_3O_4@SiO_2, Nanocomposite, 1,4Dihydroxyanthraquinone, Properties of Nanoabsorbents, Bivalent Copper, Efficient Removal, Magnetic Separation.

ABSTRACT

In this research, Fe_3O_4@SiO_2 magnetic core-shell nanoparticles functionalized with 1,4-dihydroxyanthraquinone molecules were synthesized and used to remove divalent copper ions from aqueous solutions. Then, the structural, crystalline, surface morphology, nanoparticle size, magnetic properties and thermal stability of synthetic nanoparticles were determined using Fourier transform infrared spectroscopy, X-ray diffraction, scanning electron microscope, field emission scanning electron microscope, transmission electron microscope, vibrating sample magnetometer and thermal gravimetric analysis were investigated and identified. After the synthesis of magnetic nano adsorbent, the effect of different amount of adsorbent and study of absorption kinetics in the removal of divalent copper ions was investigated and the results showed that the use of 14 mg of adsorbent leads to the removal of copper ions with a maximum absorption of 96% at ambient temperature in a period of 28 minutes and at pH 7. Finally, the recyclability and reusability of Fe_3O_4@SiO_2-DAQ in the copper ion adsorption-desorption process was investigated using a magnet and the results confirm that this synthetic nanocomposite is an effective adsorbent with excellent performance to remove divalent copper ions.

DOI: https://doi.org/10.22075/chem.2024.32798.2242

[*] **.corresponding author:** Assistant Professor of Analytical Chemistry. *E-mail address: mghahramanafshar@nri.ac.ir*

How to cite this article: Ghahraman Afshar, M., Rajabi, M., Payehghadr, M., & Bahrami Panah, N. (2024). Fe_3O_4@ SiO_2 Magnetic Core-Shell Nanoparticles Functionalized with 1, 4-dihydroxyanthraquinone as an Effective and Recyclable Adsorbent for Removal of Copper Ion from Aqueous Solutions. *Applied Chemistry Today*, **19(73)**, 123-138. (in Persian)

1. Introduction

The heavy metal ions of industrial effluents cause a major problem to human health. These kind of issues from an environmental critical situation. As a result, the necessity of heavy metal removal from the environment are particularly important [1-5]. Therefore, various physical and biological chemistry processes including reverse osmosis, filtration, biological absorption, membrane separation, ion exchange, and absorption are applied to purify water and wastewater from heavy metal ions [6-12].

Among all mentioned techniques, the adsorption technique has received much attention due to its features such as uniform and effective impact, the possibility of removing small amounts of heavy metal ions, low synthetic costs and the ability to use many biocompatible compounds. Taking high concentration of copper in the human body leads to increase heart rate, nausea, headache, blood pressure drops, ear infection, attention deficit disorder and reading and writing disorder. Moreover, deposited copper in brain and liver leads to damage of liver, lack of urine production, hair loss and anemia [13-18].

Copper poisoning have many side effects include autism symptoms such as paranoid, delusion, insanity, insomnia, depression, personality changes and schizophrenia symptoms such as lack of awareness and understanding of the five senses and time and high irritability. As a result, removing copper ion from water and wastewater sample attract much attention due to all issues caused by copper ion on the metabolism of living organisms [19-25].

Iron oxide nanoparticles especially magnetite (Fe_3O_4) have been very much considered from the point of view of theoretical and practical applications. Iron oxide nanoparticle is an attractive class of sorbent due to their unique physical properties such as low toxicity, small particles, high surface-to-volume ratio, easy separation processes by using a magnetic field and high magnetic properties. As a result, these magnetic nanoparticles have been widely used in catalysts, ion exchangers, gas sensors, magnetic resonance imaging and adsorbents [26-30].

Iron oxide nanoparticles possess a great chemical property nevertheless, these nanoparticles are dissolved easily in acidic environments. As a result, it is an unsuitable sorbent in acidic environment. Moreover, magnetite nanoparticles are oxidized when it is exposed to the atmosphere and it tend to clump due to high surface activity. In order to overcome these issues, it is necessary to use a covering and stabilizing layer to prevent surface oxidizing. For this purpose, silica cover has been applied for protecting the surface of nanomagnetic adsorbent. Silica is known as great cover for magnetic nanoparticle due to the abundance of hydroxy groups, ideal environment for connecting the desired active molecules for multiple and special applications [31-38].

Here in this work, the Fe_3O_4@SiO_2 core-shell magnetic nanoparticles are functionalized with 1 and 4-dihydroxyanthraquinone molecules (Scheme 1). Afterwards, synthetic nanoparticle is characterized as a point of the structure, crystalline, morphology and size. The magnetism and thermal stability of these synthetic nanoparticles are evaluated using Fourier transform infrared spectrometry, X-ray diffraction, transmission electron microscopy and field emission scanning, vibrating sample magnetometer and thermogravimetry analysis. Finally, copper adsorption on magnetic nanoadsorbent is investigated by optimizing the amount of adsorbent and contact time [39-43].

2. Experimental part

2.1. Materials

All chemicals are purchased from Merck and Aldrich chemical companies. The other materials are in the analytical grade and they are used without any additional purification. Fourier transform infrared (FT-IR) spectra of the samples are performed using a Shimadzu FT-IR 8300 spectrometer and tablets are fabricated from the tested samples with KBr salt. The X-ray diffraction pattern is recorded by Bruker AXS D8 device with Cu Kα radiation (λ=1.5418). Transmission electron microscope (TEM) images are obtained with a Philips EM208 transmission electron microscope with an increased voltage of 100 kV.

2.2. Instrument and equipment

Synthesized nanoparticle is dispersed in ethanol using ultrasonic vibration for 10 minutes and one drop of this emulsion is placed on a copper grid coated with carbon for TEM analysis. The morphology of synthetic nanoparticles was investigated and evaluated using a Hitachi S-4160 instrument scanning electron microscope. The magnetic properties of the particles are measured using a vibrating sample magnetometer (VSM; BHV-55). The TGA thermograms are analyzed in a Perkin Elmer machine using N_2 carrier gas and a temperature rate of 20 ºC min^{-1}. The BET analysis surface area and porosity of the catalyst are determined from the nitrogen adsorption-desorption isotherm by the Brunauer-Emmett-Teller (BET) method. The distribution pore size is determined by the Barrett-Joyner-Halenda (BJH) method. NMR spectra of the samples are recorded using a Bruker Avance DPX 500 MHz spectrometer in chloroform solvent and in the presence of trimethyl silane (TMS) as an internal reference. Elemental analysis of C, N, H, and S is performed using CHNSO analyzer model Thermofinigan Flash EA-1112. Ion concentration is calculated using inductively coupled plasma spectrometry (ICP: Varian, Vista-Pro).

2.3. Synthesis of Fe_3O_4 nanoparticle

In a common method, a mixture of $FeCl_3.6H_2O$ (1.3 g, 4.8 mmol) in 15 mL of water is added to polyvinyl alcohol (PVA15000) as a surfactant and $FeCl_2.4H_2O$ (90.0 g, 4.5 mmol). The resulting mixture is stirred for 30 minutes at 80ºC. Afterwards, hexamethylenetetramine (HMTA) (1 mol/L) is added drop by drop with vigorous stirring to produce a black solid product until pH 10. The resulting mixture is heated in a water bath for 2 hours at 60°C and the black solid product is filtered and washed with ethanol three times and then dried at 80°C for 10 hours [35].

2.4. Synthesis core-shell structure of Fe_3O_4@SiO_2

Fe_3O_4 synthetic nanoparticles (0.5 g, 2.1 mmol) in a mixture of ethanol (50 mL), distilled water (5 mL) and tetraethoxysilane (TEOS) (0.2 mL) is dispersed. Afterwards, 5 mL of NaOH (10% w/w) is added drop by drop. This solution is stirred for 30 minutes at room temperature. Finally, the Fe_3O_4@SiO_2 product is separated by an external magnet and mixed with water. The obtained solution is distilled and washed three times with ethanol and dried at 80°C for 10 hours [44].

2.5. Synthesis nanoparticle of Fe_3O_4@SiO_2-NH_2 MNPs

The synthesized Fe_3O_4@SiO_2 magnetic nanoparticles (1 g) in the previous step were dispersed in 10 mL of ethanol using ultrasonic waves. Afterwards, 0.25 mL of 3-aminopropyl(triethoxy)silane (1 mmol) is added to this solution. In the next step, the resulting mixture is subjected to mechanical rotation under reflux conditions for 12 hours in order to obtain Fe_3O_4@SiO_2 nanoparticles functionalized with amine groups. In the next step, the synthetic nanoparticles are separated by applying an external magnetic field and washed several times with water

and ethanol to remove unreacted species. Finally, the synthetic nanoparticles are dried at 80°C for 6 hours [45].

2.6. Synthesis (4-hydroxy 9,10-dioxo 9,10- dihydroanthracene, 1-iloxy)-acetic acid ethyl seter (2)

A mixture of 1,4-dihydroxyanthraquinone (1 mmol), ethyl 2-bromoacetate (0.5 mmol), potassium tertiobutoxy (t-BuOK, 0.5 mmol) dissolved in 10 mL DMF solvent are subjected to mechanical rotation at room temperature for 18 hours. After the completion of the reaction (validated by TLC), 20 mL of water is added to the resulting mixture and afterwards, the mixture is filtered and dried. The obtained synthetic product (2) is purified through column chromatography using hexane/ethyl acetate (1:1/v:v) as an washing solvent. Figures 1 and 2 show the HNMR and CNMR spectra of synthetic compound (2).

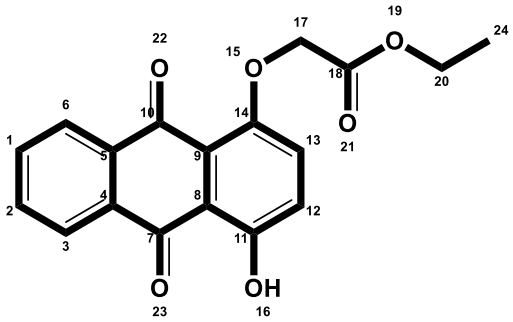

M.p. 155 ^{o}C; ^{1}H NMR (250 MHz, $CDCl_3$): δ= 1.24 (t, *J*= 7.1 Hz, 3H), 4.15-4.26 (q, 2H), 4.71 (s, 2H), 7.16 (d, *J*= 9.3 Hz, 1H), 7.30 (d, *J*= 9.3 Hz, 1H), 7.65-7.70 (m, 2H), 8.13-8.16 (m, 2H), 12.91 (s, 1H); ^{13}C NMR (62.9 MHz, $CDCl_3$): δ= 14.1 (C_{24}), 61.4 (C_{20}), 68.1 (C_{17}), 126.0 (C_8), 126.3 (C_9), 127.3 (C_{12}), 128.2 (C_3), 132.1 (C_6), 133.4 (C_{13}), 134.6 (C_1,C_2), 134.7 (C_4,C_5), 152.1 (C_{14}), 158.7 (C_{11}), 168.7 (C_{18}), 181.2 (C_{10}), 188.6 (C_7); FT-IR (KBr, Cm^{-1}): 583, 730, 786, 1023, 1054, 1105, 1165, 1205, 1356, 1427, 1592, 1636, 1666, 1734, 2995, 3439; Anal. Calcd for $C_{18}H_{14}O_6$: C, 66.26; H, 4.32%; Found: C, 66.11; H, 4.43%.

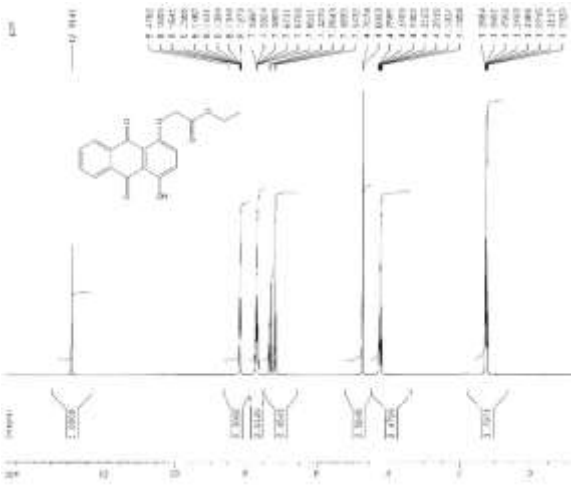

Figure 1. H-NMR spectrum of compound (2).

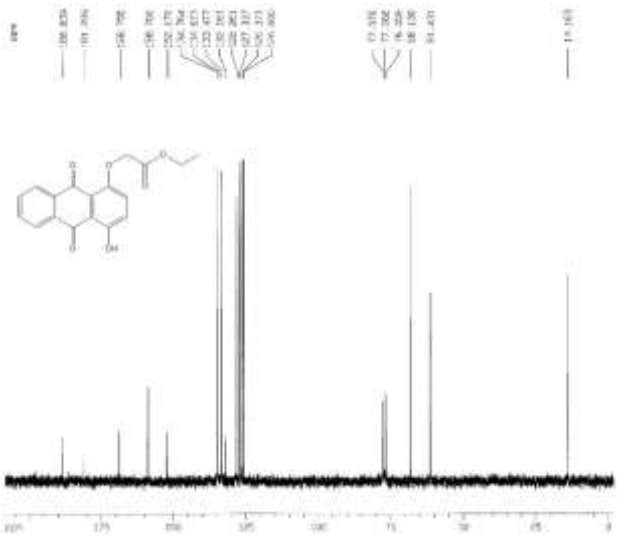

Figure 2. C-NMR spectrum of compound (2).

2.7. Synthesis of Fe_3O_4@SiO_2-DAQ nanoparticle

Surface modifications of Fe_3O_4@SiO_2-NH_2 with 4-hydroxy-9,10-dioxo-9,10-dihydroanthracene-1-yloxy)-acetic acid ethyl ester (2) is indicated in the scheme 1. This reaction is performed through the formation of a bond between the amino group and the carbonyl ester group. For this purpose, 0.5 g of Fe_3O_4@SiO_2-NH_2 nanoparticles and 1 mmol of -hydroxy-9,10-dioxo-9,10-dihydroanthracene-1-yloxy)-acetic acid ethyl ester (2) (0.325 g) dissolved in 10 mL of ethanol are mixed and subjected to mechanical rotation in order to prepare a homogeneous suspension. The reaction mixture is refluxed for 24 hours. Afterwards, Fe_3O_4@SiO_2-DAQ synthetic nanoparticles are washed several

times with ethanol and distilled water using a magnetic separation. In the next step, the obtained nanoparticle is dried in a vacuum oven at 70°C. The synthesis process of Fe_3O_4@SiO_2 nanoparticles functionalized with 1,4-dihydroxyanthraquinone is shown in scheme 1.

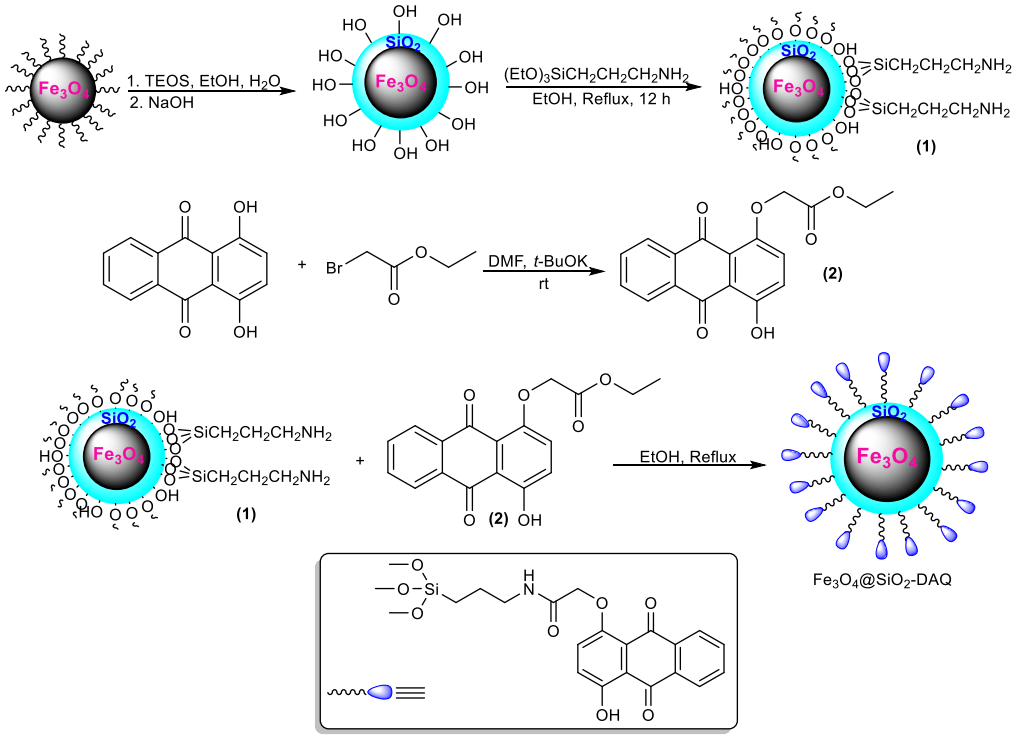

Scheme 1. Synthesis process of Fe_3O_4@SiO_2 nanoparticles functionalized with 1,4-dihydroxyanthraquinone.

2.8. Time-dependent manner of Fe_3O_4@SiO_2-DAQ in the adsorption process

Time-dependent adsorption manner of copper ions is evaluated by using 14 mg of Fe_3O_4@SiO_2-DAQ nanoadsorbent in 50 mL of copper ion solution (initial concentration of copper: 0.35 mmol/L) at ambient temperature in pH 7 within the range of 4-32 minutes. In the next step, the adsorbent nanoparticles are separated by using a magnetic separation and followed that the number of remaining ions in the solution is analyzed by using inductively coupled plasma spectroscopy (ICPMS).

3. Results and discussions

3.1. Characterization of synthetic nanoparticle

3.1.1. The FTIR spectra of synthetic nanoparticle

The infrared spectra of Fe_3O_4 nanoparticles and synthetic compounds, Fe_3O_4@SiO_2, Fe_3O_4@SiO_2-NH_2, ester (2) and Fe_3O_4@SiO_2-DAQ are shown in Figure 3. In this figure (a-f), peaks in the region of 3400 cm^{-1} and 1620 cm^{-1} is related to the stretching and bending vibrations of O-H for magnetic nanoparticles. Moreover, the peak in the region of 570 cm^{-1} is related to the Fe-O bond of the Fe_3O_4 compound. The surface of Fe_3O_4 nanoparticles is covered with silica layers. The infrared spectrum of Fe_3O_4@SiO_2 shows peaks in the region of 576 cm^{-1} (Fe-O), 807cm^{-1} (symmetric stretching vibrations Si-O-Si) and 1081cm^{-1} (asymmetric stretching vibrations Si-O-Si) shows O-H group (Figure 3b). In the FT-IR spectrum of Fe_3O_4@SiO_2-NH_2, appeared peaks in the regions of 577, 1150-1000, 1410-1400, 1546 and 2986-2810 cm^{-1} are related to Fe-O stretching vibrations, asymmetric Si-stretching vibrations. O-Si, C-N stretching vibrations, N-H bending vibrations and C-H stretching vibrations, respectively. Moreover, the peak in the region of 3165-3390 cm^{-1} is related to N–H stretching vibrations (Figure 3c) [46].The presence of absorption peaks in the region of 3031-

2878, 1734, 1665, 1476 and 1355 cm^{-1} are respectively assigned to C-H stretching vibrations, C=O (ester), C=O (ketone), CH_2 and CH_3 bending vibrations which are confirmed the synthesis process of the ester composition (2). Additionally, the peaks in the regions of 1038 and 1549 cm^{-1} are related to carbonyl groups which are created through a forming of hydrogen bond with the hydroxy group of the anthraquinone molecule [47] (Figure 3d).

The absorption peaks at 1645 and 1544 cm^{-1} are belonged to C=O stretching vibrations. amide and anthraquinone and C=O (hydrogen bond with ring hydroxy group) are presented as in 1000-1150 (Si-O-Si stretching vibrations) and 578 cm^{-1} is belonged to Fe-O stretching vibrations. All mentioned peaks prove that Fe_3O_4@SiO_2-NH_2 nanoparticles are functionalized with ester compound (2) (Figure 3 e) [48].

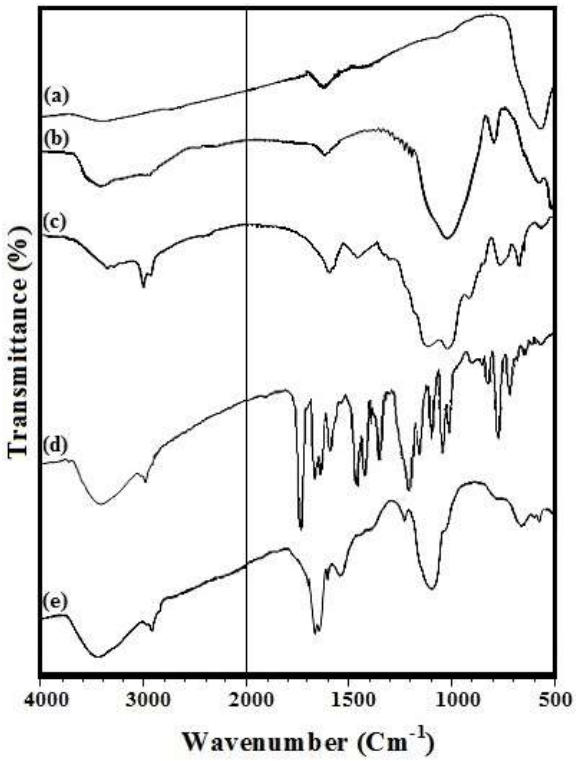

Figure 3. Fourier transform infrared spectra of (a) Fe_3O_4, (b) Fe_3O_4@SiO_2, (c) Fe_3O_4@SiO_2-NH_2, (d) ester (2) and (e) Fe_3O_4@SiO_2-DAQ.

3.1.2. X-ray diffraction spectrum (XRD)

X-ray diffraction patterns for Fe_3O_4, Fe_3O_4@SiO_2 and Fe_3O_4@SiO_2-DAQ nanoparticles are shown in Figure 4. In this figure, the diffraction peaks at 62.62º, 57º, 4.53 º, 1.43 º, 4.35 º, 1.30 º = θ2 are belonged to the Miller indices (220), (311), (400), (422), (511) and (440), respectively. These are confirmed the presence of Fe_3O_4 nucleus with crystal structures [49].

In figure (4. b, c), X-ray diffraction patterns of Fe_3O_4@SiO_2 and Fe_3O_4@SiO_2-DAQ show several diffractions this proves that peaks in the 20-70º region which are completely similar to Fe_3O_4 nanoparticles. As a result of coating the Fe_3O_4 nanoparticles with silica and the surface functionalization, the surface changes of Fe_3O_4 nanoparticles do not lead to phase change. On the other hand, the intensity of the peaks clearly decreases which indicates a broad peak related to amorphous silicate in 10º-20º region of the spectrum (Figure 4b).

In the structure of Fe_3O_4@SiO_2-DAQ nanoparticles, the broad peak is shifted to lower angles due to the interference effect of amorphous silicate and organic compounds (Figure 4c). Moreover, the average crystal particle size of Fe_3O_4 might be calculated through Scherer's equation and through peak (311). According to Scherer's equation, the calculated size of Fe_3O_4, Fe_3O_4@SiO_2 and Fe_3O_4@SiO_2-DAQ nanoparticles are equal to 11.33, 12.64 and 14.32 nm, respectively.

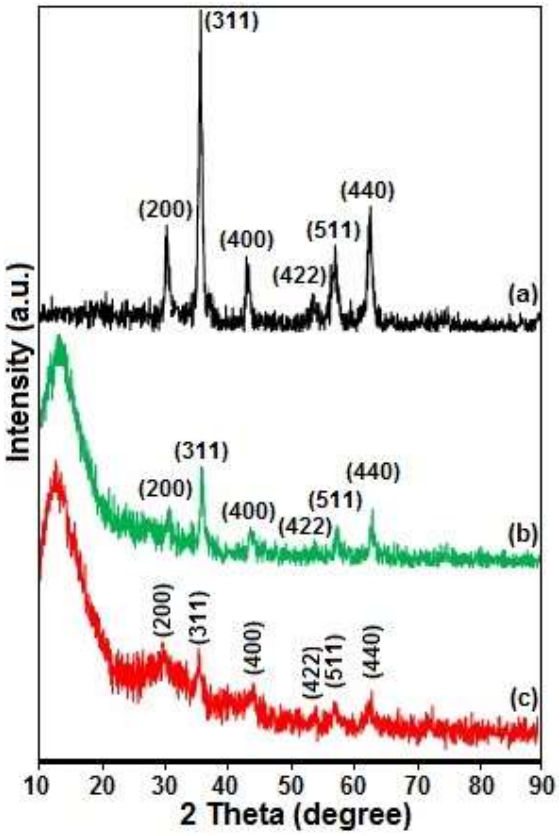

Figure 4. X-ray diffraction pattern for (a) Fe_3O_4, (b) Fe_3O_4@SiO_2 and (c) Fe_3O_4@SiO_2-DAQ nanoparticles.

3.1.3. Field emission scanning electron microscope (FE-SEM) and transmission electron microscope (TEM)

The morphology of synthetic nanoparticles of (a) Fe_3O_4 and (b) Fe_3O_4@SiO_2 and (c) Fe_3O_4@SiO_2-DAQ are investigated by using a scanning electron microscope (Figure 5). FE-SEM images show that Fe_3O_4 nanoparticles are successfully covered with silica layer and anthraquinone molecules. Moreover, these nanoparticles have almost spherical morphology.

The morphology and structures of synthetic nanoparticles are examined in different stages using a transmission electron microscope (Figure 5d-f). The TEM image reveals that the diameter of Fe_3O_4 nanoparticles is about 10 nm with uniform style (Figure 5 d). After coating the nanoparticle with silica layer, the diameter of Fe_3O_4@SiO_2 increases to about 20 nm and the thickness of the silica layer is approximately equal to 10 nm (Figure 5-3 e). Moreover, the TEM image indicates that Fe_3O_4@SiO_2-DAQ nanoparticles are spherical in shape with an approximate diameter of 55 nm (Figure 5 f).

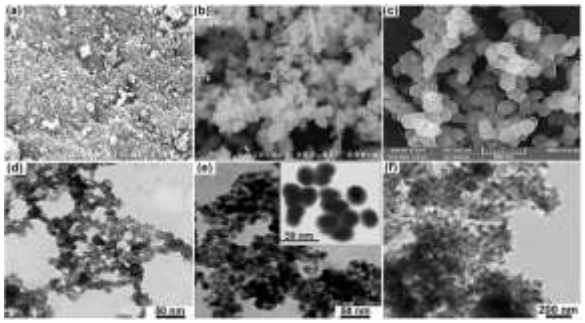

Figure 5. FE-SEM images of (a) Fe_3O_4, (b) Fe_3O_4@SiO_2 and (c) Fe_3O_4@SiO_2-DAQ using same magnification. TEM images of (d) Fe_3O_4, (e) Fe_3O_4@SiO_2 and (f) Fe_3O_4@SiO_2- nanoparticles. DAQ.

3.1.4. Vibrating magnetometer analysis (VSM)

The magnetic properties of Fe_3O_4, Fe_3O_4@SiO_2 and Fe_3O_4@SiO_2-DAQ nanoparticles are investigated using a vibrating sample magnetometer at room temperature (Figure 6A). The results indicates that the saturation magnetization value for Fe_3O_4, Fe_3O_4@SiO_2 and Fe_3O_4@SiO_2-DAQ nanoparticles is 64.8, 40.3 and 32.7 mu/g, respectively. It is clear that the amount of saturation magnetization of Fe_3O_4 nanoparticles decreases gradually with the increase of silica and anthraquinone ligand. These superparamagnetic nanoparticles have permanent diamagnetic moments in the absence of external magnetic field. However, superparamagnetic nanoparticles indicate their magnetic responsibility in the presence of a magnetic field. (Figure 6B).

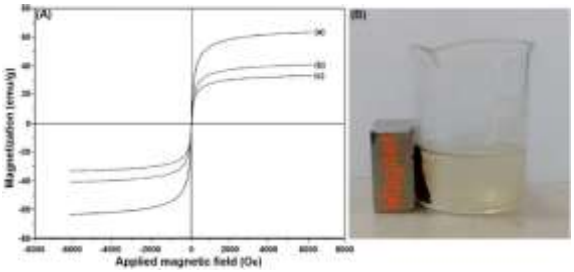

Figure 6. Magnetic curves at 300ºK for nanoparticles of (a) Fe_3O_4, (b) Fe_3O_4@SiO_2 and (c) Fe_3O_4@SiO_2-DAQ, (B) separation process of Fe_3O_4@SiO_2-DAQ using a magnetic magnet.

3.1.5. Thermogravimetric analysis (TGA)

Thermogravimetric analysis of Fe_3O_4@SiO_2 and Fe_3O_4@SiO_2-DAQ nanoparticles are performed in a temperature range of 50-700ºC (Figure 7). These nanoparticles show two stages of weight loss in this temperature range. The reduction below 200°C is related to the removal of solvent or water while the secondary weight loss stage at higher temperature than 200°C is related to the decomposition of organic compounds on a magnetic substrate [50].

According to Figure 7a, the weight loss in the range of 50-200°C is related to the evaporation of water and ethanol for surface absorption Fe_3O_4@SiO_2 nanoparticles. On the other hand, the weight loss in the range of 200-560°C is belonged to the release of water in the structure of nanoparticles or conversion to Fe_2O_3. The TGA curve for Fe_3O_4@SiO_2-DAQ nanoparticles shows an initial weight loss of 6.7% below 200°C, which is due to the removal of water molecules from the surface hydroxy groups. Moreover, the weight loss of about 22.4% in the range of 200-700ºC is due to the decomposition of organic compounds on the surface of nanoparticles (Figure 7b).

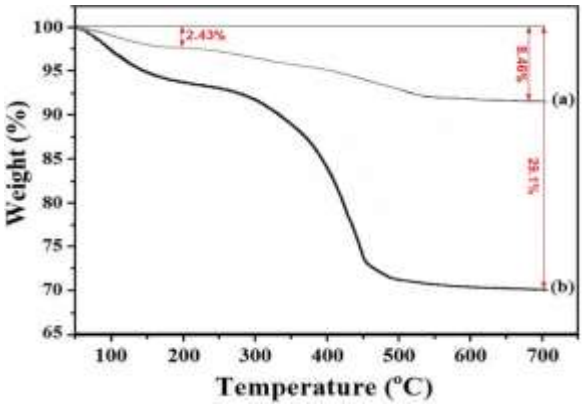

Figure 7. Thermal decomposition analysis of nanoparticles (a) Fe_3O_4@SiO_2 and (b) Fe_3O_4@SiO_2-DAQ.

3.1.6. Inductively Coupled Plasma (ICP)

By drawing the intensity curve of the spectral lines obtained from the inductively coupled plasma device, the concentration of the elements is easily determined according to the concentration of the desired element (calibration curve). In this way, it is possible to detect and measure the concentration of the desired element. Therefore, inductively coupled plasma analysis is applied to determine the residual amount of divalent copper in the solution and the amount of absorption by the Fe_3O_4@SiO_2-DAQ nanoadsorbent.

3.1.7. Analysis of nitrogen adsorption isotherms (BET)

Since the surface area of nanoparticles in the synthesized sample is not unique and constant, the roughness of the surface has a significant effect on determining the exact size of the surface. As a result, the optimal measurement of the nanoparticle surface has certain complications which affect the surface area calculation. Therefore, the specific nanoparticles size is calculated more than the expected value. Experimentally, the surface area of nanoparticles is obtained by analyzing nitrogen or other gas adsorption isotherms by using the BET analysis.

In the present study, the specific surface area and pore diameter of synthetic nanoparticles are calculated by using BET and BJH methods. The results show that the specific surface area for Fe_3O_4, Fe_3O_4@SiO_2 and Fe_3O_4@SiO_2-DAQ nanoparticles are 480, 430 and 378 m^2/g, respectively. (Table 1)

Table 1. BET results of Fe_3O_4, Fe_3O_4@SiO_2 and Fe_3O_4@SiO_2-DAQ nanoparticles.

No	Sample	Specific surface area (m^2/g)	Pore volume (cm^3/g)	Average pore diameter (nm)
1	Fe_3O_4	480	0.803	1.254
2	Fe_3O_4@SiO_2	430	0.755	1.787
3	Fe_3O_4@SiO_2-DAQ	378	0.741	1.896

3.2. Performance investigation of $Fe_3O_4@SiO_2$-DAQ nanoparticle in copper adsorption

3.2.1. Effect of adsorbent dosage amount on adsorption performance

The adsorption behaviour is depended on the amount of $Fe_3O_4@SiO_2$-DAQ nanoadsorbent in copper ion solution. For this purpose, the initial concentration of 0.3 mmol/L of copper ion is applied to investigate the adsorbent dosage at ambient temperature, pH 7 with a contact time of 22 minutes. Afterwards, various amounts of adsorbent in the range of 2 to 16 mg in 50 mL of copper solution are subjected in order to evaluate the adsorption capacity. According to the obtained results, the maximum adsorption capacity is obtained by using 14 mg of adsorbent. On the other hand, higher amounts of adsorbent (16 mg) do not show an impact on the absorption rate (Figure 8 a). The major characteristics of nanostructured materials is known as a high extraction efficiency, fast kinetics and low adsorbent consumption are. The increase in removal efficiency up to 14 mg is due to the increase in available absorbent sites. Due to the constant concentration of copper, increasing the amount of adsorbent more than 14 mg does not show any effect on the amount of absorption.

3.2.2. Effect of contact time on adsorption performance

The time decency behaviour of $Fe_3O_4@SiO_2$-DAQ adsorbent is investigated in the absorption of copper ion in the range of 4 to 32 minutes at the initial concentration of 0.35 mmol/L and ambient temperature. The amount of adsorption significantly increases with increasing contact time up to 28 minutes which leads reaching the adsorption capacity of 96%. However, the longer contact time (32 minutes) does not have an effect on the progress of metal ion adsorption (Figure 8b). The presence of active heteroatomic groups with high coordination power leads high surface-to-volume ratio of the synthetic nanoadsorbent. This active site leads increasing the penetration of copper ions in the free surfaces in solid-liquid interactions. As a result, the main reasons for the excellent performance of this adsorbent are obtained. Moreover, increasing the contact time decreases the absorption rate due to the decrease in the concentration of the remaining ions in the solution and saturating the adsorbent sites (Figure 8b).

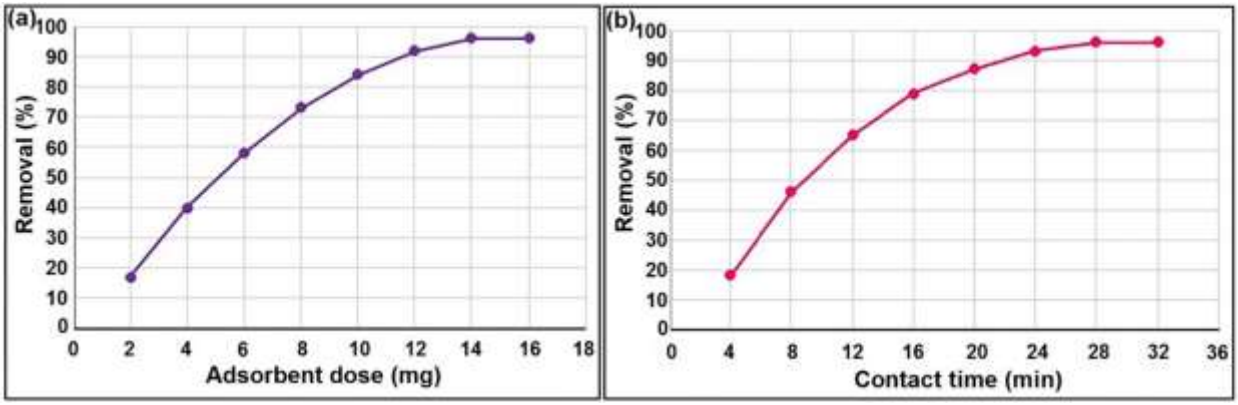

Figure 8. (a) Optimizing the amount of adsorbent in copper ion removal, (b) Investigating the effect of time on the amount of adsorbent absorption.

3.2.3. Ability to recycle and reuse adsorbent

Reusability and regeneration of adsorption capacity is a critical factor for any advanced adsorbent. High adsorption capacity and excellent desorption properties count as two prominent features of these adsorbents. High adsorption-desorption rate has a significant effect on reducing the overall cost of the extraction process. Therefore, the recovery and reusability of $Fe_3O_4@SiO_2$-DAQ is investigated in

the adsorption of copper ion under optimal adsorption-desorption conditions.

The results show that after 6 times of recovery and use of this adsorbent, a noticeable decrease in adsorption capacity and activity is observed. According to the results, the excellent performance and stability is obtained for nanoadsorbent after successive cycles (Figure 9). After performing each adsorption process, the nanoadsorbent is separated using a magnet, washed with hydrochloric acid (1 mol/liter) at ambient temperature to desorb copper ions. Afterwards, the nanoadsorbent is dried at 60°C and used for successive absorption-desorption process.

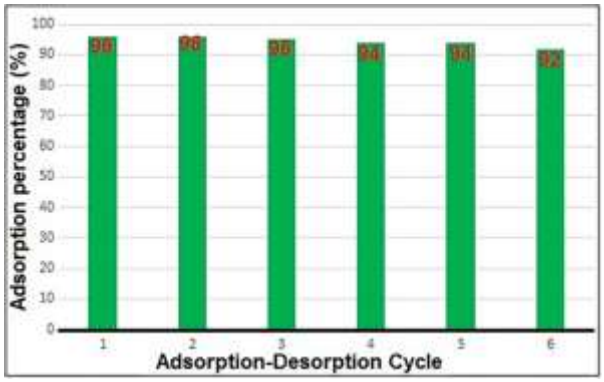

Figure 9. Recyclability and reusability of adsorbent in consecutive adsorption-desorption cycles.

3.2.4. Comparison of adsorbents

In order to compare the efficiency of the synthesized nanoadsorbent with previous methods, its maximum adsorption capacity is compared with the sorbents reported in previous studies (Table 2). According to the results, it is found that the maximum adsorption capacity of copper on the synthetic nanoadsorbent is 75.5 mg/g which provides the high value of adsorption capacity compared to previous studies. Moreover, the synthetic nanoadsorbent has features such as high absorption speed, excellent coordination power with metal, small amounts of adsorbent, the ability to separate with a magnetic field and reuse in successive cycles of absorption-desorption without a serious decrease in activity. These broad range of excellent properties makes this adsorbent suitable and efficient for solid phase extraction area.

Table 2. Comparison of the maximum adsorption capacity of various adsorbents with Fe_3O_4@SiO_2-DAQ adsorbent for copper ion removal.

Adsorbent	Adsorption capacity(q_m) (mg/g)	Ref.
Iron oxide NPs	19.3	[51]
Multi-amine-grafted mesoporous silicas	1.0	[52]
MWCNTs–IDA	6.6	[53]
Purolite Arsen X^{np}	5.6	[54]
magnetite nanorods	40.0	[55]
dairy manure biochar	54.4	[56]
iron oxide coated sewage sludge	17.3	[57]
iron oxide nanoparticles-immobilized-sand	5.81	[58]
activated charcoal derived from coffe	38.2	[59]
Fe_3O_4@SiO_2-DAQ NPs	75.5	Presented

4. Conclusion

In this research, Fe_3O_4@SiO_2 core-shell nanoparticles functionalized with anthraquinone molecules are synthesized and its performance in effective removal of divalent copper from aqueous solutions is investigated. The results indicate that this nanoadsorbent exhibits excellent performance in removing metal ions in a short period of time with high adsorption capacity. This nanoparticle possesses a high porosity, surface-active heteroatomic groups with high coordination power and high surface-to-volume ratio. Moreover, this nanoadsorbent is able to be applied for several adsorption-desorption cycle s and reused for 6 times without a serious decrease in adsorption capacity.

5. Acknowledgments

Authors gratefully acknowledge the financial support of this work by the Research Council of

Payame Noor University of Karaj and Niroo Research Institute.

5. References

[1] Das, P.N., Jithesh, K., and Raj, K.G. (2021). Recent developments in the adsorptive removal of heavy metal ions using metal-organic frameworks and graphene-based adsorbents. *Journal of the Indian Chemical Society*, 98(11), 100188.

[2] Esmaeilpour, M ,.Larimi, A., Asgharinezhad, A., Ghahramanafshar, M., and Faghihi, M. (2022). Silica nanoparticles extracted from rice husk and functionalized with dendrimer as an effective recyclable adsorbent to remove divalent cadmium from aqueous solutions. *Journal of Applied Research of Chemical-Polymer Engineering*, 6(1), 63-76.

[3] Guo, X., Feng, Q., Fan, D., Wang, Z., Ren, Y., Sun, B., and Yang, D. (2022). An agent-based dynamic reliability modeling method for multistate systems considering fault propagation: A case study on subsea Christmas trees. *Process Safety and Environmental Protection*, 158, 20-33.

[4] Soleimani, M., Ghaderi, S., Afshar, M.G., and Soleimani, S. (2012). Synthesis of molecularly imprinted polymer as a sorbent for solid phase extraction of bovine albumin from whey, milk, urine and serum. *Microchemical Journal*, 100, 1-7.

[5] Afshar, M.G., Tercier-Waeber, M., Wehrli, B., and Bakker, E. (2017). Direct sensing of total alkalinity profile in a stratified lake. *Geochem. Perspect. Lett*, 3(1), 85-93.

[6] Hojamberdiev, M., Daminova, S.S., Kadirova, Z.C., Sharipov, K.T., Mtalo, F., and Hasegawa, M. (2018). Ligand-immobilized spent alumina catalyst for effective removal of heavy metal ions from model contaminated water. *Journal of Environmental Chemical Engineering*, 6(4), 4623-4633.

[7] Safir, I., Ngo, K.X., Abraham, J.N., Afshar, M.G., Pavlova, E., and Nardin, C. (2015). Synthesis and structure formation in dilute aqueous solution of a chitosan-DNA hybrid. *Polymer*, 79, 29-36.

[8] Zeng, T., Yu, Y., Li, Z ,.Zuo, J., Kuai, Z., Jin, Y., Wang, Y., Wu, A., and Peng, C. (2019). 3D MnO2 nanotubes@ reduced graphene oxide hydrogel as reusable adsorbent for the removal of heavy metal ions. *Materials Chemistry and Physics*, 231, 105-108.

[9] Asgharinezhad, A.A., Esmaeilpour, M., and Afshar, M.G. (2024). Synthesis of magnetic Fe3O4@ SiO2 nanoparticles decorated with polyvinyl alcohol for Cu (II) and Cd (II) ions removal from aqueous solution. *Chemical Papers*, 1-16.

[10] Esmaeilpour, M. and Ghahraman Afshar, M. (2023). Magnetic Nanoadsorbent: Preparation, characterization, and Adsorption Properties for Removal of Copper (II) from Aqueous Solutions. *Applied Chemistry Today*, 18(69), 11-20.

[11] Niknam, E., Naffakh-Moosavy, H., Moosavifard, S.E., and Afshar, M.G. (2022). Amorphous V-doped Co3S4 yolk-shell hollow spheres derived from metal-organic framework for high-performance asymmetric supercapacitors. *Journal of Alloys and Compounds*, 895, 162720.

[12] Afshar, M.G., Crespo, G.A., and Bakker, E. (2015). Thin-Layer Chemical Modulations by a Combined Selective Proton Pump and pH

Probe for Direct Alkalinity Detection. *Angewandte Chemie*, 127(28), 8228-8231.

[13] Barkade, S., Sable, S., Ashtekar, V., and Pandit, V. (2022). Removal of lead and copper from wastewater using Bael fruit shell as an adsorbent. *Materials Today: Proceedings*, 53, 65-70.

[14] Gupta, V. and Nayak, A. (2012). Cadmium removal and recovery from aqueous solutions by novel adsorbents prepared from orange peel and Fe2O3 nanoparticles. *Chemical engineering journal*, 180, 81-90.

[15] Soleimani, M., Ghahraman Afshar, M., and Sedghi, A. (2013). Amino-functionalization of multiwall carbon nanotubes and its use for solid phase extraction of mercury ions from fish sample. *International Scholarly Research Notices*, 2013.

[16] Wang, L., Hu, D., Kong, X., Liu, J., Li, X., Zhou, K., Zhao, H., and Zhou, C. (2018). Anionic polypeptide poly (γ-glutamic acid)-functionalized magnetic Fe3O4-GO-(o-MWCNTs) hybrid nanocomposite for high-efficiency removal of Cd (II), Cu (II) and Ni (II) heavy metal ions. *Chemical engineering journal*, 346, 38-49.

[17] Esmaeilpour, M., Ghahraman Afshar, M., and Ghaseminejad, H. (2024). Investigation of water consumption in Shahid Montazer Ghaem steam Power Plant and technical-economic evaluation of the boilers' blowdown recycling solutions. *Nashrieh Shimi va Mohandesi Shimi Iran*, 42(4), 177-189.

[18] Soleimani, M., Mahmodi, M.S., Morsali, A., Khani, A., and Afshar, M.G. (2011). Using a new ligand for solid phase extraction of mercury. *Journal of hazardous materials*, 189(1-2), 371-376.

[19] Emenike, E.C., Adeniyi, A.G., Omuku, P.E., Okwu, K.C., and Iwuozor, K.O. (2022). Recent advances in nano-adsorbents for the sequestration of copper from water. *Journal of Water Process Engineering*, 47, 102715.

[20] Esmaeilpour, M., Ghahraman Afshar, M., and Kazemnejadi, M. (2023). Preparation, characterization, and adsorption properties of bis-salophen schiff base ligand immobilized on Fe3O4@ SiO2 nanoparticles for removal of lead (II) from aqueous solutions. *Applied Chemistry*, 18(66), 125-146.

[21] Khalil, N.A., Rahman, A.S.A., Huraira, A.M.A., Janurin, S.N.D.F., Fizal, A.N.S., Ahmad, N., Zulkifli, M., Hossain, M.S., and Yahaya, A.N.A. (2023). Magnetic chitosan hydrogel beads as adsorbent for copper removal from aqueous solution. *Materials Today: Proceedings*, 74, 499-503.

[22] Ghahraman Afshar, M., Esmaeilpour, M., and Ghaseminejad, H. (2024). Microbial corrosion affected by environmental factors in cooling tower of Bandar Abbas power plant. *Journal of Environmental Studies*, 49(4), 389-400.

[23] Niknam, E., Naffakh-Moosavy, H., and Afshar, M.G. (2022). Electrochemical performance of Nickel foam electrode in Potassium Hydroxide and Sodium Sulfate electrolytes for supercapacitor applications. *Journal of Composites and Compounds*, 4(12), 149-152.

[24] Zandbaaf, S., Khorrami, M.R.K., and Afshar, M.G. (2022). Genetic algorithm based artificial neural network and partial least

squares regression methods to predict of breakdown voltage for transformer oils samples in power industry using ATR-FTIR spectroscopy. *Spectrochimica Acta Part A: Molecular and Biomolecular Spectroscopy*, 273, 120999.

[25] Soleimani, M., Afshar, M.G., and Ganjali, M.R. (2013). High selective methadone sensor based on molecularly imprinted polymer carbon paste electrode modified with carbon nanotubes. *Sensor Letters*, 11(10), 1983-1991.

[26] Esmaeilpour, M., Ghahraman Afshar, M., Noroozi Tisseh, Z., and Ghahremanzadeh, R. (2023). Removal of copper and chromium ions from aqueous solutions with magnetic nanoparticles functionalized with N-phosphonomethyl amino diacetic acid. *Journal of Applied Research of Chemical-Polymer Engineering*, 7(1), 33-46.

[27] Javidi, J., Esmaeilpour, M., and Khansari, M.R. (2015). Synthesis, characterization and application of core–shell magnetic molecularly imprinted polymers for selective recognition of clozapine from human serum. *Rsc Advances*, 5(89), 73268-73278.

[28] Miller, M., Prinz, G., Cheng, S.-F., and Bounnak, S. (2002). Detection of a micron-sized magnetic sphere using a ring-shaped anisotropic magnetoresistance-based sensor: A model for a magnetoresistance-based biosensor. *Applied Physics Letters*, 81(12), 2211-2213.

[29] Hanifehpour, Y., Mirtamizdoust, B., and Golbedaghi, R. (2024). Synthesis, characterization and X-ray crystal structure of a new cocrystal complex of and preparation the related nano cadmium (II) oxide. *Applied Chemistry Today*, 19(71), 9-22.

[30] Niknam, E., Naffakh-Moosavy, H., Moosavifard, S.E., and Afshar, M.G. (2021). Multi-shelled bimetal V-doped Co3O4 hollow spheres derived from metal organic framework for high performance supercapacitors. *Journal of Energy Storage*, 44, 103508.

[31] Aghayee, M., Zolfigol, M.A., Keypour, H., Yarie, M., and Mohammadi, L. (2016). Synthesis and characterization of a novel magnetic nano-palladium Schiff base complex: application in cross-coupling reactions. *Applied Organometallic Chemistry*, 30(8), 612-618.

[32] Asgharinezhad, A.A.A., Esmaeilpour, M., and Afshar, M.G. (2023). Synthesis of magnetic Fe3O4@ SiO2 nanoparticles decorated with polyvinyl alcohol for heavy metal ion removal from aqueous solution.

[33] Chen, X., Zhu, J., Chen, Z., Xu, C., Wang, Y., and Yao, C. (2011). A novel bienzyme glucose biosensor based on three-layer Au–Fe3O4@ SiO2 magnetic nanocomposite. *Sensors and Actuators B: Chemical*, 159(1), 220-228.

[34] Esmaeilpour, M. and Ghahraman Afshar, M. (2023). Magnetic Nanoadsorbent: Preparation, characterization, and Adsorption Properties for Removal of Copper (II) from Aqueous Solutions. *Applied Chemistry*.

[35] Esmaeilpour, M., Javidi, J., Dehghani, F., and Dodeji, F.N. (2014). Fe 3 O 4@ SiO 2–imid–PMA n magnetic porous nanospheres as recyclable catalysts for the one-pot synthesis of 14-aryl-or alkyl-14 H-dibenzo [a, j] xanthenes and 1, 8-dioxooctahydroxanthene derivatives

under various conditions. *New Journal of Chemistry*, 38(11), 5453-5461.

[36] Esmaeilpour, M., Larimi, A., Ghahramanafshar, M., and Faghihi, M. (2023). Ethylenediaminetetraacetic acid coated Fe_3O_4@ SiO_2 nanocomposite: An effective adsorbent for the removal of copper ions from aqueous system. *Applied Chemistry*, 17(65), 45-54.

[37] Hossienzadeh, M., Hassanpour, A., AliHosseini, M., Safardoust, H., and Mirzaei, M. (2024). Synthesis and Characterization of NiO/ZnO Nanocomposite and its Application in Ibuprofen Drug Delivery. *Applied Chemistry Today*, 19(71), 69-80.

[38] Néel, B., Ghahraman Asfhar, M., Crespo, G.A., Pawlak, M., Dorokhin, D., and Bakker, E. (2014). Nitrite-Selective Electrode Based On Cobalt (II) tert-Butyl-Salophen Ionophore . *Electroanalysis*, 26(3), 473-480.

[39] Asgharinezhad, A.A., Esmaeilpour, M., and Afshar, M.G. (2024). Synthesis of magnetic Fe3O4@ SiO2 nanoparticles decorated with polyvinyl alcohol for Cu (II) and Cd (II) ions removal from aqueous solution. *Chemical Papers*, 78(6), 3799-3814.

[40] Ghahraman Afshar, M., Payehghadr, M., Bahrami Panah, N., and Akbari, M. (2024). Fe3O4@SiO2 magnetic core-shell nanoparticles functionalized with 1,4-dihydroxyanthraquinone as an effective and recyclable adsorbent for the removal of divalent nickel from aqueous solutions. *Iranian Chemical Engineering Journal*.- ,

[41] Kaamyabi, S., Karimi Hajishoreh, N., and akbarzadeh, a. (2024). Design of termo-sensitive molecularly imprinted polymers(MIP) and in vitro evaluation of controlled release of Eptifibatide drug. *Applied Chemistry Today*, 19(71), 81-94.

[42] Afshar, M.G., Azimi, M., Habibi, N., Masihi, H., and Esameilpour, M. (2023). Batch and continuous bleaching regimen in the cooling tower of Montazer Ghaem power plant. *Journal of Hazardous Materials Advances*, 11, 100339.

[43] Niknam, E., Ghahraman Afshar, M., Ghaseminejad, H., and Esamaeilpour, M. (2022). Pharmaceutical Pollutants Removal by Using Electrochemical Oxidation Technique. *Journal of Water and Wastewater; Ab va Fazilab (in persian)*, 33(4), 71-81.

[44] Deng, Y., Qi, D., Deng, C., Zhang, X., and Zhao, D. (2008). Superparamagnetic high-magnetization microspheres with an Fe3O4@ SiO2 core and perpendicularly aligned mesoporous SiO2 shell for removal of microcystins. *Journal of the American Chemical Society*, 130(1), 28-29.

[45] Dindarloo Inaloo, I., Majnooni, S., Eslahi, H., and Esmaeilpour, M. (2020). Nickel (II) nanoparticles immobilized on EDTA-modified Fe3O4@ SiO2 nanospheres as efficient and recyclable catalysts for ligand-free Suzuki–Miyaura coupling of aryl carbamates and sulfamates. *ACS omega*, 5(13), 7406-7417.

[46] Sardarian, A.R., Kazemnejadi, M., and Esmaeilpour, M. (2019). Bis-salophen palladium complex immobilized on Fe 3 O 4@ SiO 2 nanoparticles as a highly active and durable phosphine-free catalyst for Heck and copper-free Sonogashira coupling reactions. *Dalton Transactions*, 48(9), 3132-3145.

[47] Bloom, H., Briggs, L., and Cleverley, B. (1959). 33. Physical properties of anthraquinone and its derivatives. Part I. Infrared spectra. *Journal of the Chemical Society (Resumed)*, 178-185.

[48] Sharghi, H., Beyzavi, M.H., Safavi, A., Doroodmand, M.M., and Khalifeh, R. (2009). Immobilization of porphyrinatocopper nanoparticles onto activated multi-walled carbon nanotubes and a study of its catalytic activity as an efficient heterogeneous catalyst for a click approach to the three-component synthesis of 1, 2, 3-triazoles in water. *Advanced Synthesis & Catalysis*, 351(14-15), 2391-2410.

[49] Huang, X., Wang, G., Yang, M ,.Guo, W., and Gao, H. (2011). Synthesis of polyaniline-modified Fe3O4/SiO2/TiO2 composite microspheres and their photocatalytic application. *Materials Letters*, 65(19-20), 2887-2890.

[50] Zarnegar, Z. and Safari, J. (2014). Fe 3 O 4@ chitosan nanoparticles :a valuable heterogeneous nanocatalyst for the synthesis of 2, 4, 5-trisubstituted imidazoles. *Rsc Advances*, 4(40), 20932-20939.

[51] Banerjee, S.S. and Chen, D.-H. (2007). Fast removal of copper ions by gum arabic modified magnetic nano-adsorbent. *Journal of hazardous materials*, 147(3), 792-799.

[52] Zhang, L., Yu, C., Zhao, W., Hua, Z., Chen, H., Li, L., and Shi, J. (2007). Preparation of multi-amine-grafted mesoporous silicas and their application to heavy metal ions adsorption. *Journal of Non-Crystalline Solids*, 353(44-46), 4055-4061.

[53] Wang, J., Ma, X., Fang, G., Pan, M., Ye, X., and Wang, S. (2011). Preparation of iminodiacetic acid functionalized multi-walled carbon nanotubes and its application as sorbent for separation and preconcentration of heavy metal ions. *Journal of hazardous materials*, 186(2-3), 1985-1992.

[54] Kołodyńska, D., Kowalczyk, M., and Hubicki, Z. (2014). Evaluation of iron-based hybrid materials for heavy metal ions removal. *Journal of Materials Science*, 49, 2483-2495.

[55] Karami, H. (2013). Heavy metal removal from water by magnetite nanorods. *Chemical engineering journal*, 219, 209-216.

[56] Xu, X., Cao, X., Zhao, L., Wang, H., Yu, H., and Gao, B. (2013). Removal of Cu, Zn, and Cd from aqueous solutions by the dairy manure-derived biochar. *Environmental Science and Pollution Research*, 20, 358-368.

[57] Phuengprasop, T., Sittiwong, J., and Unob, F. (2011). Removal of heavy metal ions by iron oxide coated sewage sludge. *Journal of hazardous materials*, 186(1), 502-507.

[58] Lee, S.-M., Laldawngliana, C., and Tiwari, D. (2012). Iron oxide nano-particles-immobilized-sand material in the treatment of Cu (II), Cd (II) and Pb (II) contaminated waste waters. *Chemical engineering journal*, 195, 103-111.

[59] Yeung, P.-T., Chung, P.-Y ,.Tsang, H.-C., Tang, J.C.-O., Cheng, G.Y.-M., Gambari, R., Chui, C.-H., and Lam, K.-H. (2014). Preparation and characterization of bio-safe activated charcoal derived from coffee waste residue and its application for removal of lead and copper ions. *Rsc Advances*, 4(73), 38839-38847.